Supporting Information

Spatially isolating Li^+ reduction from Li deposition via $Li_{22}Sn_5$ alloy protective layer for advanced Li metal anode

Jia Xie,[ac] Jing Xue,*[b] Hongyi Wang[a] and Jingze Li*[ac]

[a] Yangtze Delta Region Institute (Huzhou), University of Electronic Science and Technology of China, Huzhou 313001, P. R. China.

[b] School of Mathematics and Physics, Weinan Normal University, Weinan 714099, PR China

[c] School of Materials and Energy, University of Electronic Science and Technology of China, Chengdu 611731, P. R. China.

E-mail: jingxuewnu@163.com; lijingze@uestc.edu.cn

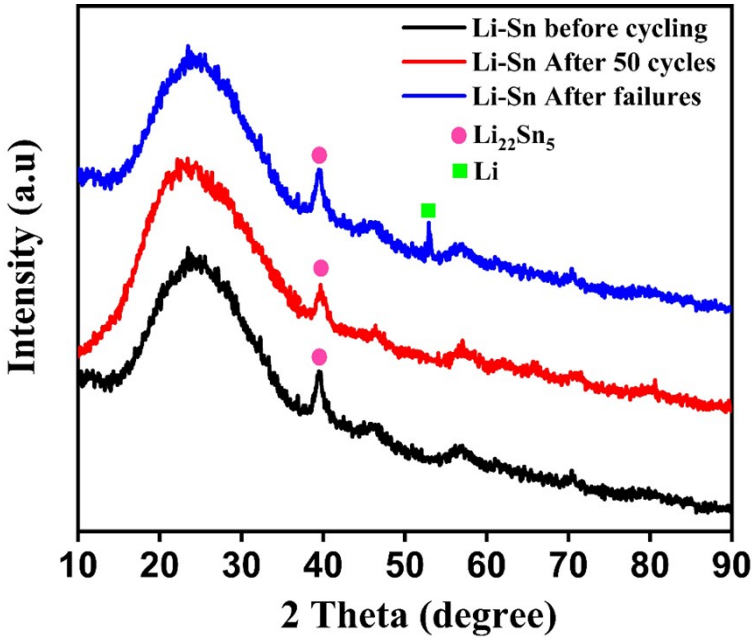

Figure S1. XRD profiles of the Li-Sn alloy layers detached by the adhesive tape from the coated Li foil metal after various cycles.

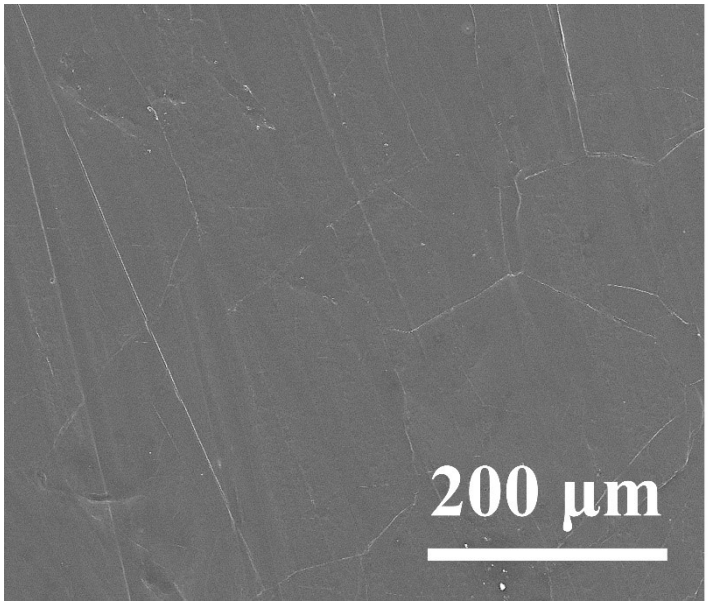

Figure S2. SEM image of the Li-Sn alloy protective layer fabricated by sputtering of Sn on Li foil and the subsequent alloying reaction between Sn and Li.

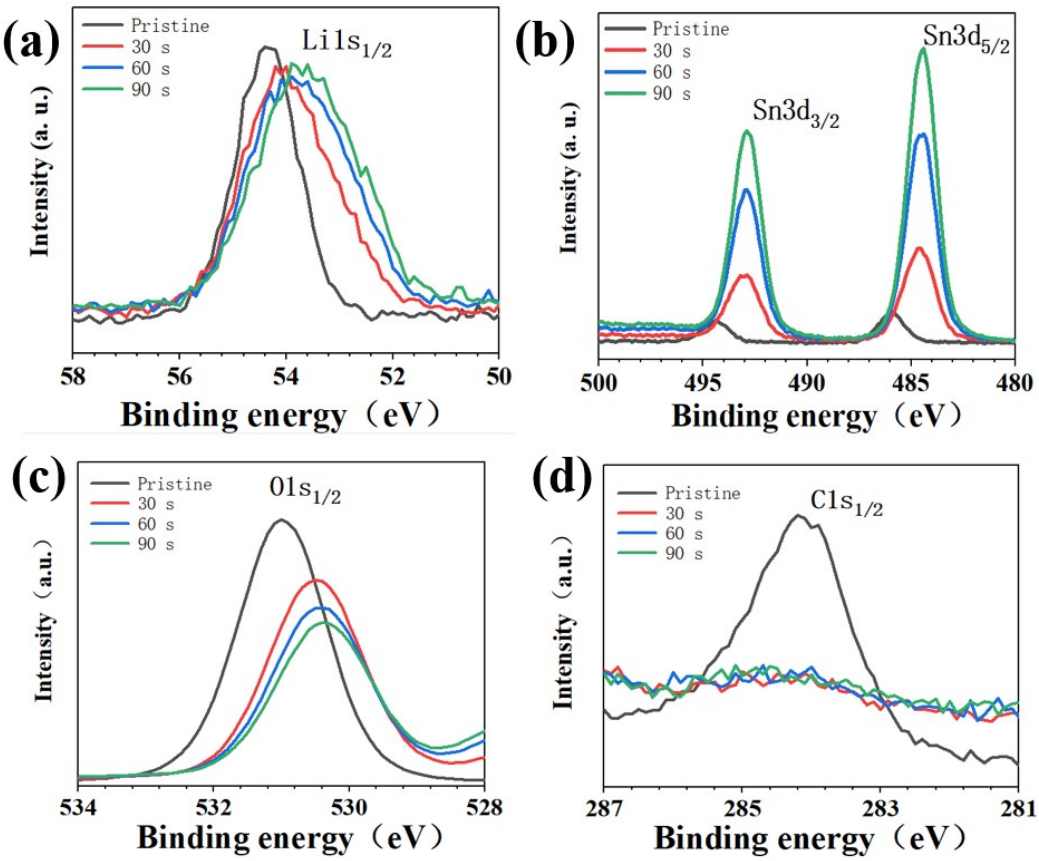

Figure S3. XPS spectra of Sn coated Li anode which was etched by ion beam for 0, 30, 60 and 90 s. (a) O1s; (b) Sn3d; (c) O1s; (d) C1s.

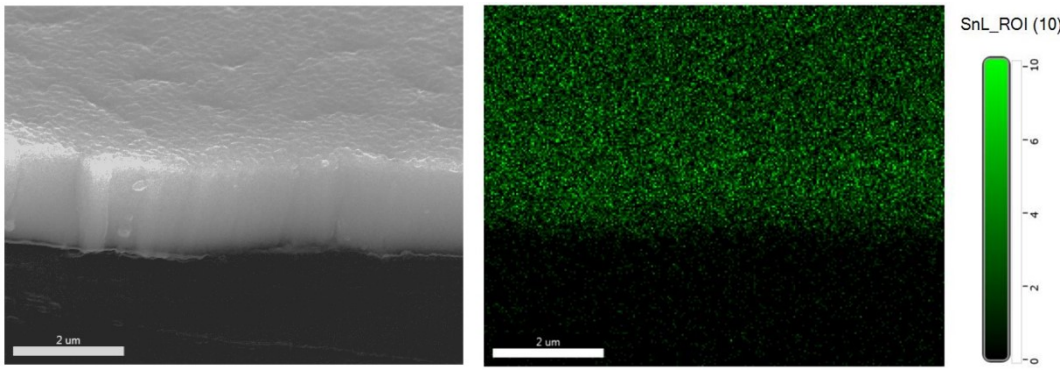

Figure S4. Side-view SEM image (left) and the corresponding EDS mapping image recorded in the vertical direction.

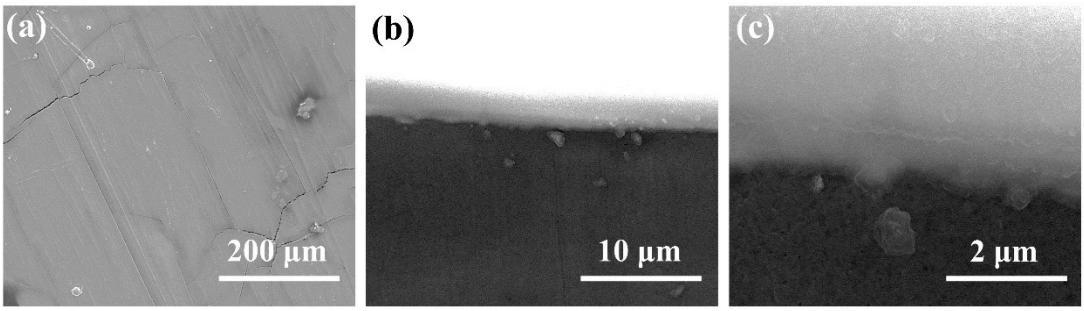

Figure S5. Top-view (a) and side-view (b-c) SEM images of the Li-Sn@Li electrode in the 1st Li plating process at 0.1 mA cm^{-2} and 0.5 mA h cm^{-2}.

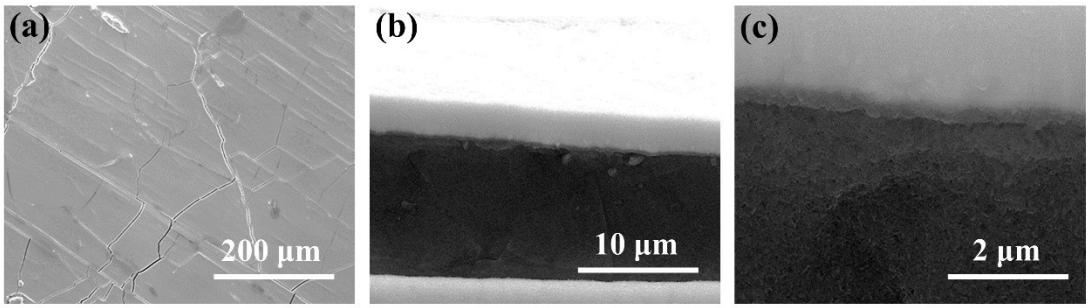

Figure S6. Top-view (a) and side-view (b-c) SEM images of the Li-Sn@Li electrode in the 1st Li plating process at 0.5 mA cm^{-2} and 1 mA h cm^{-2}.

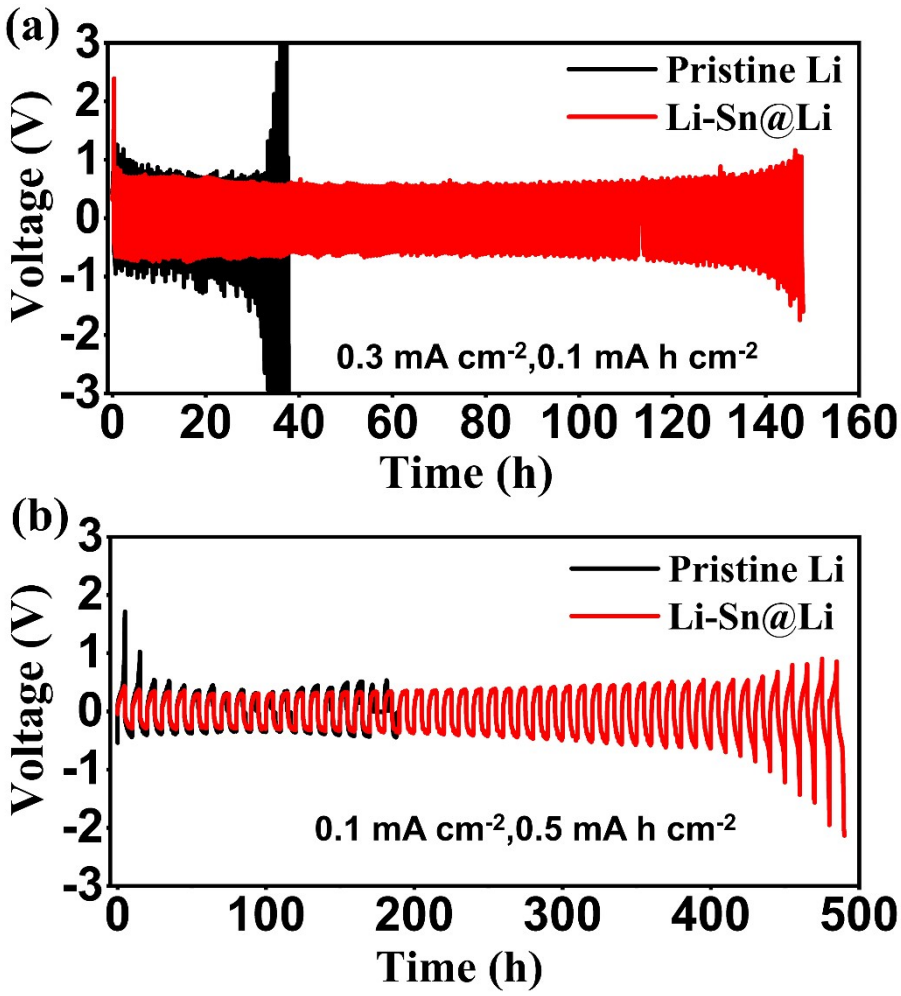

Figure S7. Cycling performance of Li/Li and Li-Sn@Li/Li-Sn@Li symmetric cells at (a) 0.3 mA cm^{-2} and 0.1 mA h cm^{-2}; (b) 0.1 mA cm^{-2} and 0.5 mA h cm^{-2}.

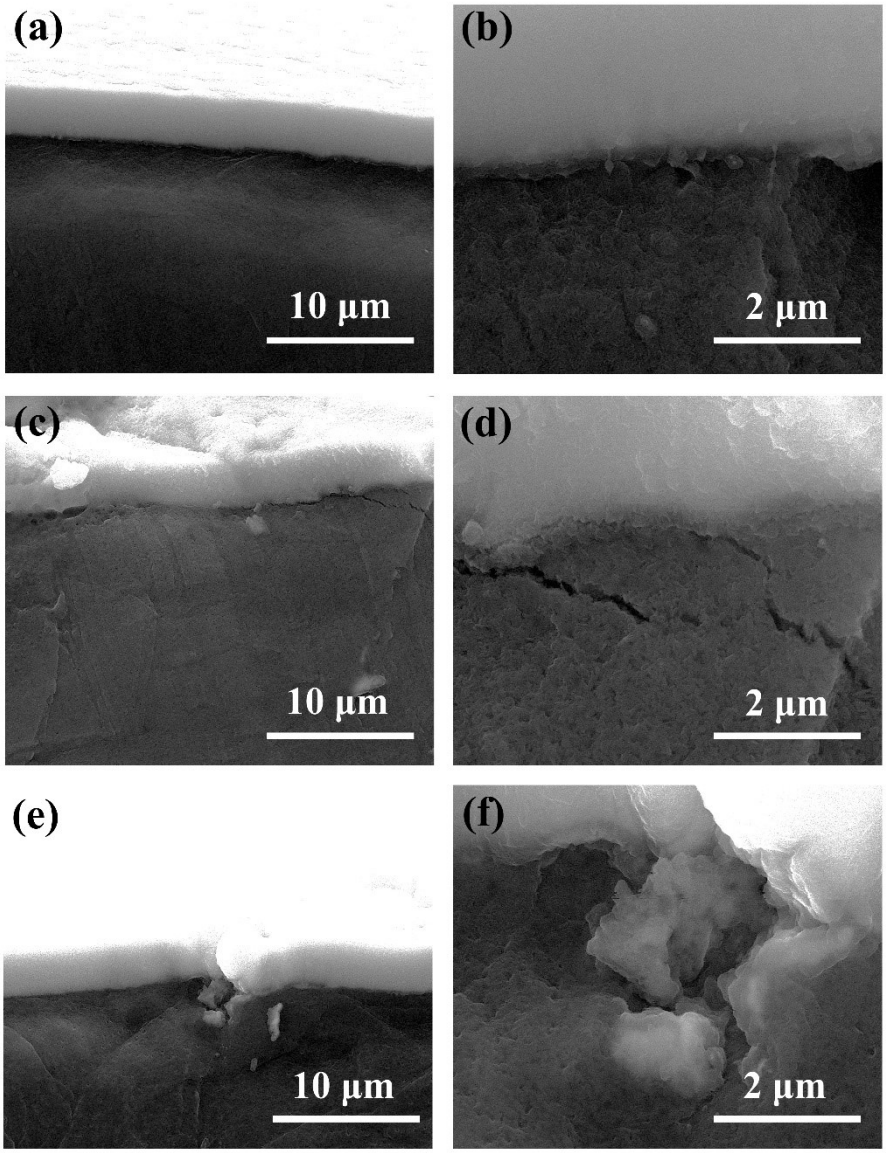

Figure S8. Side-view SEM images of the Li-Sn@Li electrode after 50 cycles at (a-b) 0.1 mA cm^{-2} and 0.1 mA h cm^{-2}; (c-d) 0.5 mA cm^{-2} and 0.5 mA h cm^{-2}; (e-f) 1 mA cm^{-2} and 1 mA h cm^{-2}.

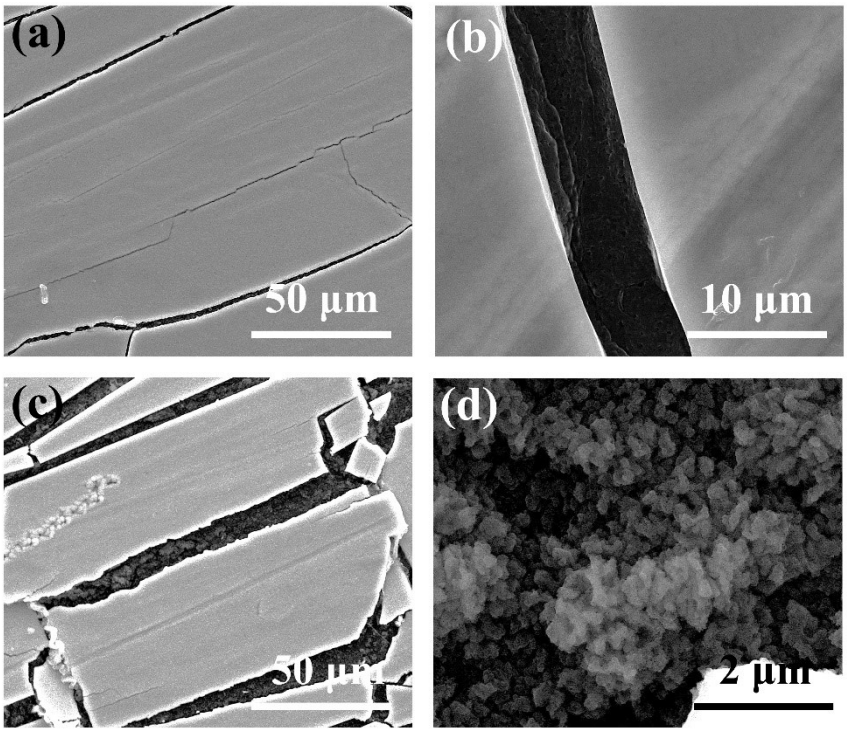

Figure S9. SEM images of the Li-Sn@Li electrode at 0.1 mA cm^{-2} and 0.5 mA h cm^{-2} after (a-b) 20 cycles and (c-d) 40 cycles.

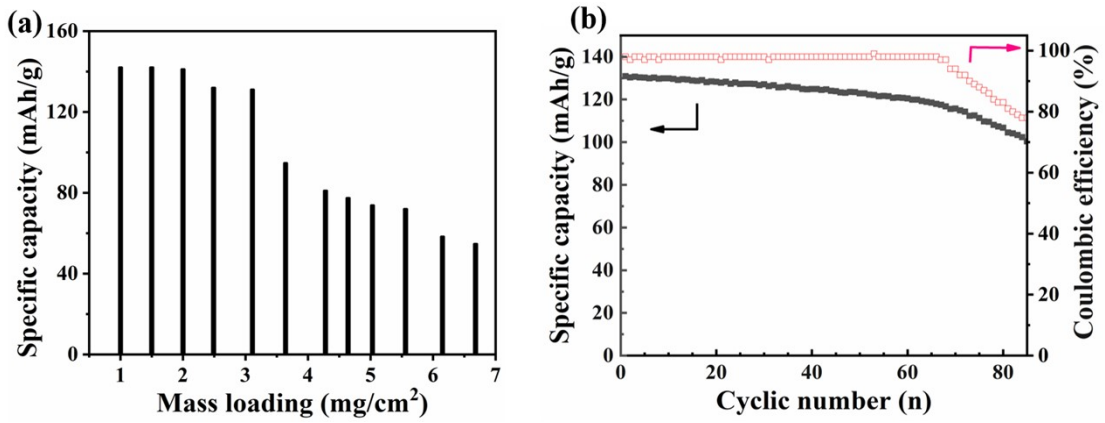

Figure S10. (a) The specific discharge capacity as a function of LFP mass loading; (b) The cyclic performance of LFP based full cell with the active material mass loading of 3.1 mg/cm^2.

Table S1. The performance comparison among the symmetric cells with the modified Li anodes and solid state electrolytes.

Symmetrical cells	Current density ($mA\ cm^{-2}$)	Areal capacity ($mA\ h\ cm^{-2}$)	Temperature (°C)	Lifespan (h)	Ref.
Li/PEO-SCN-LLZTO/Li	0.2	0.1	60	50	[1]
Li/PEO-SCN-LAGP/Li	0.2	0.2	40	250	[2]
Li/PEO-SCN/Li	0.1	0.1	25	450	[3]
Li/PEO-SCN-GF/Li	0.1	0.1	25	500	[4]
Li-Ag/LLCZNO/Li-Ag	0.2	0.1	25	100	[5]
Li-Mg/ LLZO /Li-Mg	0.1	0.02	25	37	[6]
Li-Si/PEO/Li-Si	0.5	0.5	60	1000	[7]
Li-Ge/LAGP/Li-Ge	0.1	0.1	25	200	[8]
$LiCa_2$-LiFe/LLZTO/$LiCa_2$-LiF	0.1	0.1	25	1000	[9]
Li-Al-Si/LLZTO/Li-Al-Si	0.1	0.1	25	1500	[10]
Li-Sn@Li/PEO-SCN/Li-Sn@Li	0.1	0.1	25	1300	This work
	0.1	0.5	25	500	This work

References

[1] Zha, W.; Chen, F.; Yang, D.; Shen, Q.; Zhang, L. High-performance $Li_{6.4}La_3Zr_{1.4}Ta_{0.6}O_{12}$/poly(ethylene oxide)/succinonitrile composite electrolyte for solid-state lithium batteries. Journal of Power Sources 2018, 397, 87-94. https://doi.org/10.1016/j.jpowsour.2018.07.005

[2] Peng, J.; Wu, L.-N.; Lin, J.-X.; Shi, C.-G.; Fan, J.-J.; Chen, L.-B.; Dai, P.; Huang, L.; Li, J.-T.; Sun, S.-G. A solid-state dendrite-free lithium-metal battery with improved electrode interphase and ion conductivity enhanced by a bifunctional solid plasticizer. Journal of Materials Chemistry A 2019, 7, 19565-19572. https://doi.org/10.1039/c9ta07165b

[3] Xu, S.; Sun, Z.; Sun, C.; Li, F.; Chen, K.; Zhang, Z.; Hou, G.; Cheng, H. M.; Li, F. Homogeneous and fast ion conduction of peo-based solid-state electrolyte at low temperature. Advanced Functional Materials 2020, 30. https://doi.org/10.1002/adfm.202007172

[4] Wang, J.; Yang, J.; Shen, L.; Guo, Q.; He, H.; Yao, X. Synergistic effects of plasticizer and 3D framework toward high-performance solid polymer electrolyte for room-temperature solid-state lithium batteries. ACS Applied Energy Materials 2021, 4, 4129-4137. https://doi.org/10.1021/acsaem.1c00468

[5] Feng, W.; Dong, X.; Li, P.; Wang, Y.; Xia, Y. Interfacial modification of Li/garnet electrolyte by a lithiophilic and breathing interlayer. Journal of Power Sources 2019, 419, 91-98. https://doi.org/10.1016/j.jpowsour.2019.02.066

[6] Fu, K. K.; Gong, Y.; Fu, Z.; Xie, H.; Yao, Y.; Liu, B.; Carter, M.; Wachsman, E.; Hu, L. Transient behavior of the metal interface in lithium metal-garnet batteries. Angewandte Chemie-International Edition 2017, 56, 14942-14947. https://doi.org/10.1002/anie.201708637

[7] Zhou, F.; Li, Z.; Lu, Y. Y.; Shen, B.; Guan, Y.; Wang, X. X.; Yin, Y. C.; Zhu, B. S.; Lu, L. L.; Ni, Y.; Cui, Y.; Yao, H. B.; Yu, S. H. Diatomite derived hierarchical

hybrid anode for high performance all-solid-state lithium metal batteries. Nature Communication 2019, 10, 2482. https://doi.org/ 10.1038/s41467-019-10473-w
[8] Liu, Y.; Li, C.; Li, B.; Song, H.; Cheng, Z.; Chen, M.; He, P.; Zhou, H. Germanium thin film protected lithium aluminum germanium phosphate for solid-state Li batteries. Advanced Energy Materials 2018, 8, 1702374. https://doi.org/10.1002/ aenm.201702374
[9] Wei, J.; Yang, Z.; Li, Z.; Lu, G; Xu, C. Constructing a composite lithium anode for high-performance solid-state lithium–metal batteries via in-situ alloying reaction. Functional Materials Letters 2022, 15(03): 2250015. https://doi.org/10.1142/ S1793604722500151
[10]Zhai, L.; Yang, K.; Jiang, F.; Liu, W.; Yan, Z.; Sun, J. High-performance solid-state lithium metal batteries achieved by interface modification. Journal of Energy Chemistry 2023, 79, 357-364. https://doi.org/ 10.1016/j.jechem.2023.01.022

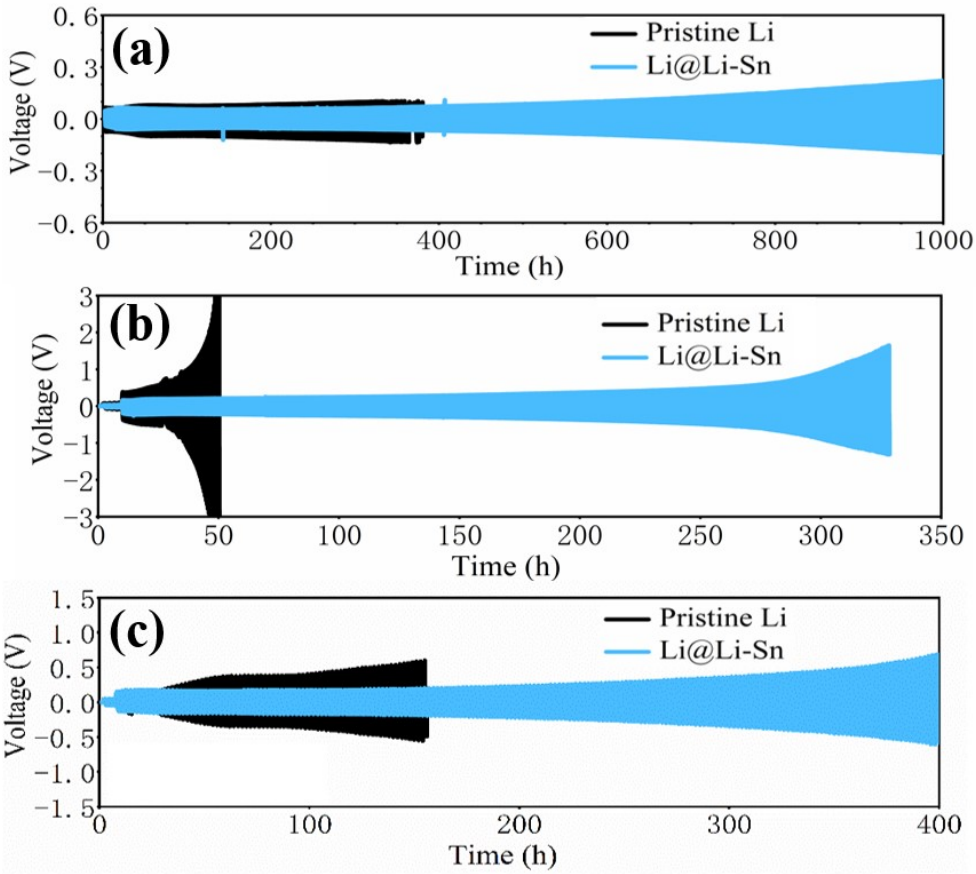

Figure S11. Cycling performance of symmetric cells of Li/Li and Li-Sn@Li/Li-Sn@Li under 60 °C at (a) 0.1 mA cm^{-2} and 0.1 mAh cm^{-2}, (b) 0.5 mA cm^{-2} and 0.1 mAh cm^{-2}, (c) 0.3 mA cm^{-2} and 0.3 mA h cm^{-2}.